journal of the mechanical behavior of biomedical materials 143 (2023) 105880

Contents lists available at ScienceDirect

Journal of the Mechanical Behavior of Biomedical Materials

journal homepage: www.elsevier.com/locate/jmbbm

Ultraviolet light induces mechanical and structural changes in full thickness human skin

Abraham Ittycheri, Zachary W. Lipsky, Tracy A. Hookway, Guy K. German *

Department of Biomedical Engineering, Binghamton University, State University of New York, Binghamton, NY, USA

A B S T R A C T

While the detrimental health effects of prolonged ultraviolet (UV) irradiation on skin health have been widely accepted, the biomechanical process by which photoaging occurs and the relative effects of irradiation with different UV ranges on skin biomechanics have remained relatively unexplored. In this study, the effects of UV-induced photoageing are explored by quantifying the changes in the mechanical properties of full-thickness human skin irradiated with UVA and UVB light for incident dosages up to 1600 J/cm^2. Mechanical testing of skin samples excised parallel and perpendicular to the predominant collagen fiber orientation show a rise in the fractional relative difference of elastic modulus, fracture stress, and toughness with increased UV irradiation. These changes become significant with UVA incident dosages of 1200 J/cm^2 for samples excised both parallel and perpendicular to the dominant collagen fiber orientation. However, while mechanical changes occur in samples aligned with the collagen orientation at UVB dosages of 1200 J/cm^2, statistical differences in samples perpendicular to the collagen orientation emerge only for UVB dosages of 1600 J/cm^2. No notable or consistent trend is observed for the fracture strain. Analyses of toughness changes with maximum absorbed dosage reveals that no one UV range is more impactful in inducing mechanical property changes, but rather these changes scale with maximum absorbed energy. Evaluation of the structural characteristics of collagen further reveals an increase in collagen fiber bundle density with UV irradiation, but not collagen tortuosity, potentially linking mechanical changes to altered microstructure.

1. Introduction

Exposure to ultraviolet (UV) light offers health benefits to human skin including vitamin D production (Moan et al., 2008) and phototherapy for treating skin conditions like atopic eczema (Reynolds et al., 2001) by limiting the growth of certain cells through UV-induced apoptosis (Morita et al., 1997). However, prolonged UV exposure can also impair skin health through carcinogenesis (Böni et al., 2002), premature aging (Panich et al., 2016), and impaired wound healing (Amaro-Ortiz et al., 2014). Visible, infrared irradiation (IR), and UV induced changes in skin physiology have been previously established, linking the exposure to enhanced stimulation of fibroblast activity (Lee et al., 2006), changes in pigmentation and skin surface temperature (Kollias and Baqer, 1984), and secretion of catabolic enzymes like matrix metalloproteinases (MMP) by dermal cells such as fibroblasts (Cho et al., 2009; Chung et al., 2002; Fisher et al., 1996). Prior studies note that MMP catabolic enzymes have been known to break down one or more components of the dermal extracellular matrix (ECM). Enzymes including interstitial collagenase can cleave types I, II, and III collagen fibers (Welgus et al., 1985) while a variant of macrophage metalloelastase (EC 3.4.24.65) has been noted to target all major components of the dermal ECM, except for type I collagen (Chandler et al., 1996). Due to its higher photonic energy, the impact of UV light on cellular, tissue, and biofilm behavior and physiology has been more commonly explored than other light ranges (Cho et al., 2009; Chung et al., 2002; Fisher et al., 1996; Kappes et al., 2006; Kollias and Baqer, 1984; Lee et al., 2006), however prior studies of changes in skin mechanical properties with UV irradiation widely vary, with some reporting increased fragility (Schatrffetter-Kochanek, 1996) and others reporting a more leathery like appearance (Poon et al., 2015), suggestive of tougher tissue. To date, a conclusive link between mechanical changes and prolonged UV exposure has not been established.

UV light can be separated into four ranges based on their wavelength: UVA (315–400 nm), UVB (280–315 nm), UVC (100–280 nm), and vacuum UV (100–200 nm). UVC and vacuum UV light are absorbed by the outer atmosphere (United Nations Environment Programme, 1998). However, there exist numerous sources of UVC light including biosafety cabinet sterilization bulbs, welding equipment, and the plethora of devices that claim to disinfect surfaces and air from pathogens, including SARS-CoV-2 virus (Freeman et al., 2022). Recent studies have revealed that UVA, UVB, and UVC light can all cause biomechanical degradation in human stratum corneum, the outermost layer of skin, due to the dispersion of cell-cell junction proteins away from their typical intercellular locations (Lipsky and German, 2019). However, no

* Corresponding author.
E-mail address: ggerman@binghamton.edu (G.K. German).

https://doi.org/10.1016/j.jmbbm.2023.105880
Received 12 January 2023; Received in revised form 7 March 2023; Accepted 30 April 2023
Available online 6 May 2023
1751-6161/© 2023 Elsevier Ltd. All rights reserved.

studies to date have explored the biomechanical impact of prolonged UV irradiation on full-thickness skin.

Skin is the body's largest organ and offers the first line of physical defense against most foreign insults. A simplified structural organization of the skin comprises the superficial epidermis, and the underlying dermis and hypodermis. The epidermis plays an important role in limiting the penetration of UV rays deep into the dermis, as approximately 80% of UVC, 62% of UVB, and 45% of UVA light is attenuated or reflected by the outer epidermis (Diffey, 1983). The ECM composition of the dermal layer is primarily fibrous proteins of collagen and elastin with an amorphous ground substance in between, containing glycosaminoglycans (Brown TM and Krishnamurthy K, 2021). Of the described components of the dermal ECM, collagen fibers constitute 75–80% of the dry skin mass (Silver et al., 2001; Wilkes et al., 1973), with a greater presence of types I and III collagen fibers (Brown TM and Krishnamurthy K, 2021), with a ratio of 4:1 (Brown et al., 2011). As such, collagen fibers play an important role in supporting the skin's structural integrity, although elastin fibers contribute to the skin's elasticity. The non-uniform anisotropic characteristics of the skin microstructure was first recognized in the 19th century (Langer, 1861) and was supported by mechanical testing observations, which noted a relationship between loading direction relative to the collagen orientation and the stiffness of the skin (Liang and Boppart, 2010; Ní Annaidh et al., 2012; Ridge and Wright, 1966). In order to ensure that anisotropy is considered, this study accounts for the orientation of the collagen fibers during mechanical testing and evaluates both the effects of prolonged UVA and UVB irradiation on the mechanical properties of full thickness skin and the collagen microstructure in the reticular dermis. With prior studies reporting that incident dosages of UVA, UVB, and UVC light greater than 800 J/cm^2 are required to cause degradation of human stratum corneum (Lipsky and German, 2019), this study considers dosages ranging between 800 and 1600 J/cm^2. Although differences in the mechanical properties of skin between photoexposed and photoprotected regions have been reported (Lynch et al., 2022), no study to date has explored the changes in the mechanical properties and collagen structure due to prolonged UV radiation on full-thickness skin while also considering the influence of collagen fiber orientation. This study aims to elucidate this critical knowledge gap in UV induced microstructural and mechanical changes of full thickness skin that occur with photoaging.

2. Materials and methods

2.1. Histological processing

Full-thickness skin samples were sourced from elective surgery (Yale Pathology Tissue Services, New Haven, CT) or cadavers (ConnectLife, Buffalo, NY). In total, six deidentified specimens were received for this study. The details of the specimen source, age, gender, and anatomical locations are specified in Table 1. An exempt approval (3002–13) was obtained to perform research using tissue samples pursuant to the Department of Health and Human Services (DHHS) regulations, 45 CFR 46.101:b:4. Samples were received within 24 h of surgery and within 48 h of patient mortality, Specimens then had their adipose layer fully removed are were partially sectioned, with $4 \leq n \leq 6$ samples from each specimen used for histology. The remaining tissue was used for mechanical testing.

Partially sectioned samples for histology were fixed in 10% (v/v) neutral buffered formalin (NBF) (W. W. Grainger, Inc, IL, USA) for at least 8 h. Specimens were then submerged into 30% sucrose (21H0456556, VWR, Solon, OH) and 70% 1x phosphate-buffered saline solution (PBS, K813-500 ML, AMRESCO, Cleveland, OH) for at least 12 h for cryopreservation. The samples were then embedded in a colorless sectioning medium (Neg-50™, 6502, Kalamazoo, MI) within a cryosectioning mold (4566, Tissue-TK® Cryomold®, Torrance, CA), then submerged in liquid nitrogen for 1 min until the sectioning medium was frozen. Samples were sectioned (CryoStar NX70, Thermo Scientific, Kalamazoo, MI) at −30 °C. Each section had a thickness of 10 μm. Transverse sample (plane of equal depth into the tissue) sections were acquired from the epidermis, papillary dermis, and reticular dermis, then adhered to a polarized microscopic slide (Fisherbrand™ Superfrost™ Plus Microscope Slides, 22-037-246, Fisher Scientific, Hampton, NH). Histological sections for collagen studies were established using a standard Picro Sirius Red staining method (Junqueira et al., 1979).

Table 1
Skin specimens used for the study.

Specimen Source	Specimen Age [yrs]	Specimen Sex	Skin location
ConnectLife	59	Male	Right Abdomen
Yale Pathology	66	Male	Leg
ConnectLife	90	Male	Right Abdomen
ConnectLife	67	Female	Right Abdomen
ConnectLife	92	Male	Right Abdomen
ConnectLife	68	Female	Right Abdomen

2.2. Histological imaging: collagen fiber orientation analysis

Samples were imaged using a 1x objective lens (6.45 μm/pixel, Nikon, Cfi Plan Achro Uw) on an inverted fluorescent microscope (Ti–U Eclipse, Nikon, Melville, NY) with camera (Andor Clara E, Abingdon, U. K.). The size of each sectioned dermal sample could not be fully observed within a single field of view, therefore image mosaicing was used to image the sample in its entirety (Nikon Elements, Nikon, Melville, NY). Images were analyzed for collagen fiber orientation distributions using the ImageJ Directionality tool (NIH, LOCI-University of Wisconsin-Madison) (Meijering et al., 2004; Yu et al., 2017). In addition to collagen fibers, physical gaps in the extracellular matrix (ECM) from the lamination procedure are also visible. These features can influence the overall fiber distributions, so were excluded from orientation measurements. Distributions of collagen fiber orientation appear Gaussian (Fig. 1), in agreement with previous reports (Chavoshnejad et al., 2021). Multiple sections ($3 \leq n \leq 7$) were used to establish averages and standard deviations of the collagen orientation in a sample within the vicinity (≤10 mm, notably smaller than the persistence length of Langer's lines within skin (Langer, 1861) of where samples were excised for mechanical testing. The average orientations, denoting the localized dominant collagen fiber orientation, were used to build up an orientation map within each skin specimen (Fig. 2).

Supplemental Fig. 1 depicts collagen fibers in the reticular dermis region using phase and TRITC filters.

2.3. Sample excision for mechanical studies

Using the collagen orientation map, dog bone shaped (3.2 × 35 mm) samples, were excised both parallel and perpendicular to (minimum of $n = 3$ independent samples for each orientation) the local dominant collagen fiber orientation, as shown in Fig. 2. Samples were cut using a bespoke steel die and press.

2.4. UV treatment

Samples were partially submerged in 1X PBS in a Petri dish (100 × 15 mm) to maintain consistent hydration conditions and prevent tissue drying. UV irradiation was performed in a polystyrene housing containing ice using a UV lamp (8 Watt EL Series, Analytik Jena US LLC, Upland, CA). Sample petri dishes were partially immersed in the ice with the top face of the skin samples positioned 20 mm beneath the lamp's lower face. The ice bath maintained the samples at 4 ± 2 ° C. Control samples were stored in darkness within a 4 °C refrigerator to prevent UV irradiation. To maintain consistent relative humidity conditions throughout the irradiation procedure, the polystyrene housing containing the irradiated samples and the refrigerated petri dishes

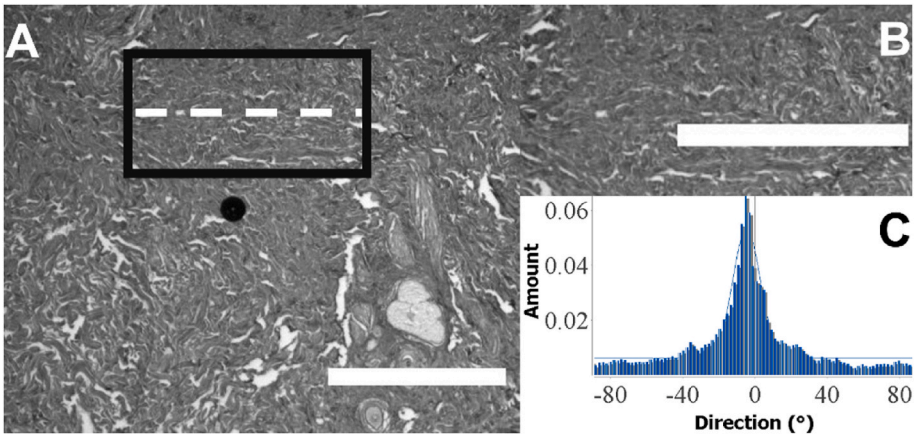

Fig. 1. Collagen Fiber Directionality Protocol. A. Orientation analysis performed on transversely sectioned sample with resolution 6.45 μm/pixel) within the reticular dermis highlighted within the black rectangle, with the white dashed line representing the dominant fiber orientation. B. A region with minimal physical gaps and high collagen volume is selected for orientation analysis using the ImageJ Directionality tool. C. Gaussian distribution of collagen fiber orientations showing a clear dominant fiber orientation. Scale bars: 1 mm.

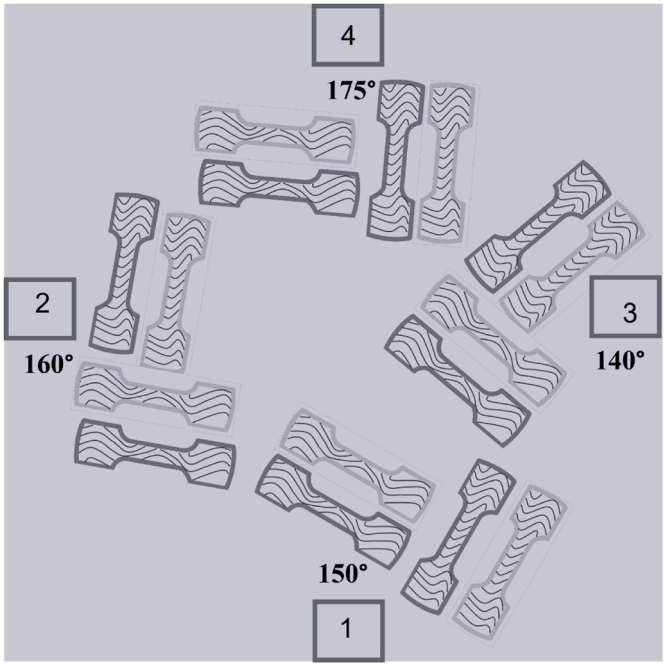

Fig. 2. Sample collagen orientation map and excision guide. Representative schematic of excision orientations at four regions of a skin specimen (regions 1–4). Dog bone samples are excised parallel and perpendicular to the local dominant collagen orientation angle (marked by the dark waves inside the dogbones). Darker shaded dog bones represent sample cuts designated for UV treatment, and lighter shaded dog bones represent sample cuts designated for control.

containing the control samples were sealed. Incident irradiation dosage time requirements for UVA (365 nm narrowband) and UVB (302 nm narrowband) irradiation were calculated based on prior light intensity measurements (Gasperini et al., 2017; Lipsky and German, 2019). Irradiation times to achieve incident dosages of UVA 800, 1200, and 1600 J/cm^2 are 58, 87, and 116 h, respectively. Irradiation times to achieve incident dosages of UVB 800, 1200, and 1600 J/cm^2 are 49, 73.5, and 98 h, respectively. To minimize confounding factors, samples irradiated for a fixed UV dosage (both parallel and perpendicular orientations) were compared with control samples from the same sample source, rested for equivalent timescales to which the corresponding samples undergo irradiation.

2.5. Tensile testing

All irradiated samples and their respective controls were rested at room temperature, partially submerged in PBS for 1 h prior to mechanical testing to equilibrate to laboratory conditions (23 °C). Subsequently, tensile testing was performed on the samples using a tensometer (UniVert, CellScale, Waterloo, ON, Canada) with 250 N load cell. Samples were mounted to the tensometer clamps and were manually stretched until a non-zero force reading at approximately 0.25 N, which is 0.1% of the load cell capacity. Then, they were strained at a constant strain rate of 10 s^{-1} until complete rupture. Tensile forces and grip separation were recorded at a frequency of 5 Hz. Force-displacement curves (Supplemental Fig. S2A) along with initial sample lengths and cross sectional areas prior to loading are processed to obtain stress-strain curves (Supplemental Fig. S2B), from which the elastic modulus, E, fracture stress, σ_f, fracture strain , ε_f, and toughness , U, were extracted . The stress-strain curves all exhibit a classic J-shaped curve with two linear regimes (Aziz et al., 2016; Chavoshnejad et al., 2021). Elastic moduli were extracted from the slope of the second linear regime of the J-shaped curve where collagen fibers are fully recruited (Aziz et al., 2016). This regime occurs at strains of $0.3 \leq \gamma \leq 1$.

3. Data analysis

3.1. Statistical analyses

Independent paired sample t-tests were performed to establish differences in the mechanical properties of irradiated samples relative to controls. Normality was first assessed using a Shapiro-Wilks test. Heteroscedasticity was measured using Levene's test. Paired, two-tail *t*-tests were performed for most statistical comparisons as a majority of the mechanical testing data had normality and equal variance. With non-normally distributed data or unequal variances, a Mann-Whitney or Welch's *t*-test were performed, respectively. RStudio was used to complete all statistical analyses (RStudio 2021.09.01, PBC, Boston, MA). Linear regression analyses were performed to evaluate changes in the mechanical properties of full thickness skin as a function of maximum absorbed energy and goodness of fit tests were applied to the linearity models to conclude statistical significance. The exclusion of outliers was guided by output from Grubbs tests. In the figures, * denotes $p \leq 0.05$, ** denotes $p \leq 0.01$, *** denotes $p \leq 0.001$, and **** denotes $p \leq 0.0001$.

3.2. Collagen structural characterization

Studies exploring UV-induced changes in the dermal collagen fiber network structure were performed on histological sections of skin specimens undergoing the greatest UVA and UVB irradiation dosages, along with their respective controls. Images acquired were used to

characterize collagen fiber density and tortuosity. Density characterizations, ρ, were quantified at depths between 1450 and 1650 μm below the base of the epidermis. Collagen fibers were imaged using an inverted microscope (Nikon) with 10x objective lens (0.59 μm/pixel, Nikon, Plan Fluor DLL, N. A. 0.3). Colour deconvolution and threshold tools within ImageJ were employed to establish a color-guided thresholding method for detecting fibers relative to the background (Yu et al., 2017), as shown in Fig. 3. Regions with minimum gaps and high collagen fiber presence were selected to avoid gaps biasing density results. Fractional density measurements were performed at a minimum of $n = 3$ regions within each section for $n = 3$ individual specimens for each treatment condition. Tortuosity characterization studies were examined using the same sections. As shown in Fig. 4, a monochromatic filter was applied to the images for improved detection of individual fibers. NeuronJ was used to trace individual collagen fibers (Meijering et al., 2004). Tortuosity was calculated by evaluating the ratio of the total length of the individually traced collagen fiber scaled by the end-to-end distance (Fig. 4C, represented as the straightness parameter, *Ps* (Rezakhaniha et al., 2012). We note that this tortuosity may not reflect the total tortuosity that exists in the fibers due to out of plane undulations. As such, these measurements constitute a conservative estimate. These snapshots of tortuosity however offer a comparable insight into the straightness parameter between UV treated and corresponding control samples. For this study, the tortuosity of $50 \leq n \leq 70$ individual collagen fibers were evaluated for each UV range and their respective controls. Skin samples used in this evaluation of collagen structural characterization were not subjected to mechanical testing.

4. Results and discussion

4.1. Changes in full-thickness skin mechanical properties with UV irradiation

Fig. 5A–D depict the average mechanical properties of full thickness skin samples irradiated with different incident dosages of UVA and UVB light, along with their respective controls. Measurements of samples excised parallel (Par.) and perpendicular (Perp.) to the dominant local collagen orientation are shown. We anticipate seeing specimen-to-specimen differences in the skin mechanical properties with anatomical site (Griffin et al., 2017), age (Lynch et al., 2022), and environment (Vierkötter and Krutmann, 2012) of the donor, and as a result, viewing monotonic global trends in Fig. 5 cannot be readily observed. Therefore, to elucidate the direct effects of UV irradiation, the fractional relative difference of the mechanical properties is taken between irradiated and corresponding control samples, both sourced from the same specimen. Fig. 6 shows the fractional relative difference of each mechanical property $(\zeta_{UV} - \zeta_C)/\zeta_C$, where ζ_{UV} denotes the measured average mechanical property after UV irradiation, ζ_C, denotes the corresponding average control value, and ζ denotes E, σ_f, ε_f, or U. Fig. 6A–C reveals that

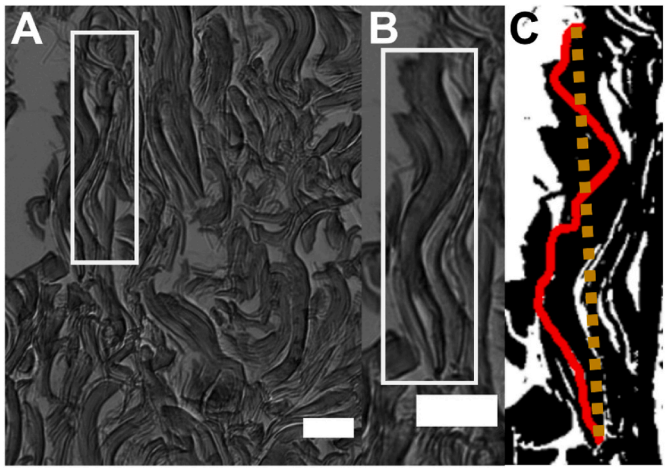

Fig. 4. Tortuosity characterization. A. Representative image of collagen fiber network (0.59 μm/pixel). The highlighted region shows an individual collagen fiber. B. Magnified image of the highlighted region in A. C. Monochromatic image of B after a filter is applied. The solid red curve and dashed brown line denote the total and end to end length of the collagen fiber, respectively. Scale bars: 50 μm.

UVA and UVB incident dosages upward of 1200 J/cm^2 result in a rise in elastic modulus, toughness, and fracture stress. Statistical changes in elastic modulus, fracture stress and toughness occur for UVA dosages of 1200 J/cm^2, both parallel and perpendicular to the collagen fiber orientation. In contrast, UVB dosages of 1200 J/cm^2 result in increases in elastic modulus, fracture stress and toughness only for samples excised parallel with the dominant collagen fiber orientation. Dosages of 1600 J/cm^2 elicit statistically significant changes in E, σ_f, and U for both orientations. No statistical difference in fracture strain occurs for any UV dosage.

While prior studies reveal UV induced mechanical degradation in the most superficial layer of the epidermis, the stratum corneum, forces required to cause sample rupture do not exceed 2 N (Lipsky and German, 2019). In contrast, forces required to rupture irradiated and unirradiated full thickness skin samples commonly exceed 200 N. As such, we do not anticipate that epidermal mechanical changes notably impact the measured mechanical changes to full thickness skin with UV irradiation.

4.2. Scaling changes in mechanical properties with absorbed UV energy

Prior studies have revealed a generalized scaling law that relates the photonic energy of UV light absorbed by human stratum corneum tissue and the degradation in its energy cost of fracture (Lipsky and German, 2019). This relationship indicates that no one UV range is more damaging than another. Rather, the magnitude of absorbed UV energy

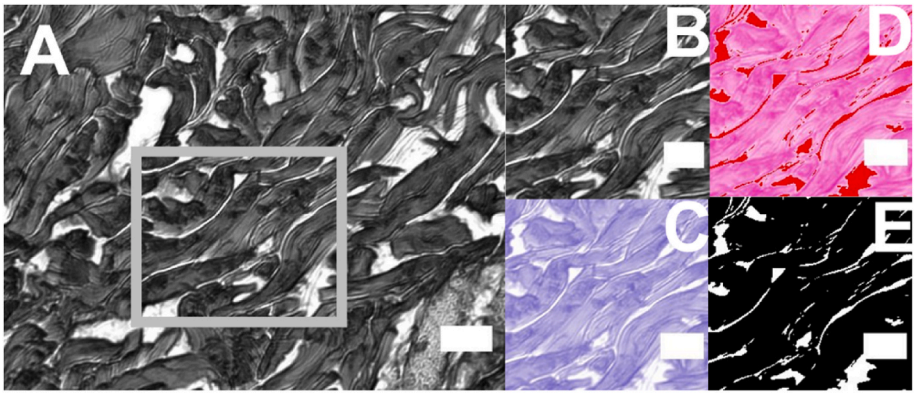

Fig. 3. Collagen density characterization. A. highlighted region (grey outline) selected from a representative image of a collagen fiber network (image resolution 0.59 μm/pixel) within the reticular dermis. B. isolated image of the highlighted region in A. C. Highlighted region from B with color deconvolution applied. D. Image from C with thresholding applied. Red regions denote gaps between collagen fibers while pink regions denote collagen. E. Monochromatic density map output from the thresholding. Dark regions denote collagen fibers while white regions denote gaps between the fibers. The measured fractional density of collagen bundles is 93.4%. Scale bars: 50 μm.

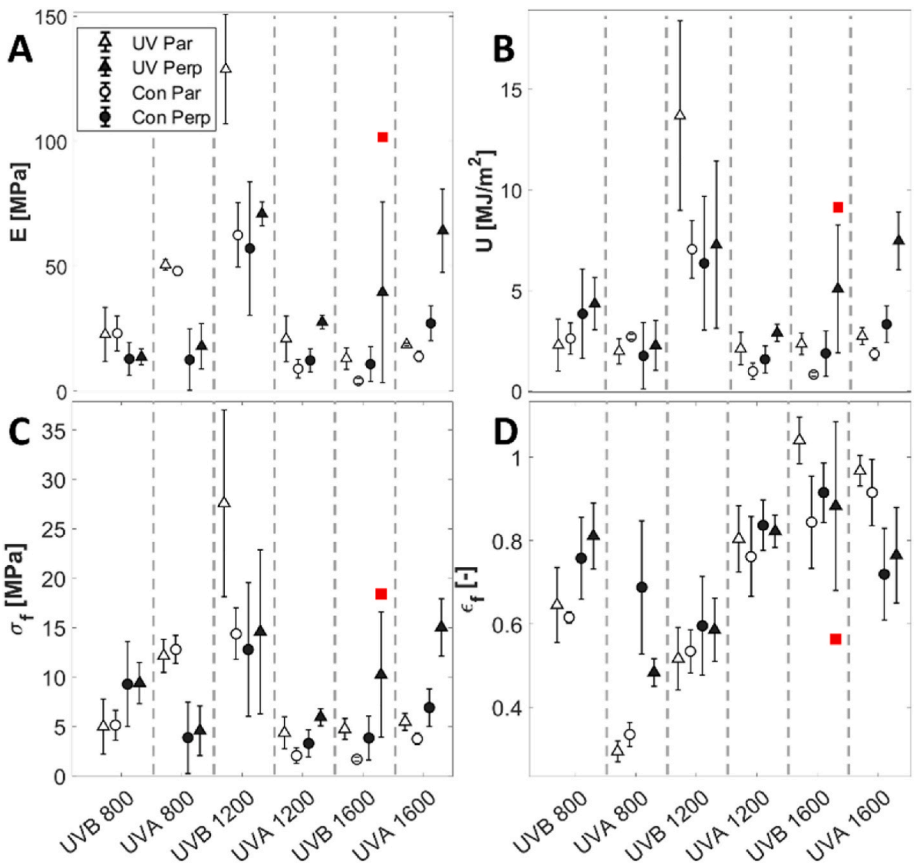

Fig. 5. Average A. elastic modulus, E, B. toughness, U, C. fracture stress, σ_f, and D. fracture strain, ϵ_f, with UVA and UVB irradiation. Results of UV irradiated samples (open symbols) and unirradiated controls (filled symbols) are shown. Samples excised parallel (triangle symbols) and perpendicular (circle symbols) to the dominant collagen fiber orientation are also presented. Bars denote averages of $3 \leq n \leq 5$ individual sample measurements for each range and dosage condition. Error bars denote standard deviations. Filled square symbols denote outliers determined by a Grubbs test with a statistical significance of $p \leq 0.05$. Vertical grey dashed lines mark the separation point between UV bandwidths and irradiation dosages.

governs the degradation of tissue mechanical integrity. To consider a similar hypothesis for dermal tissue, the amount of photonic energy transmitted to the dermis for each UV range must be quantified. Table 2 shows the total fraction of UVA and UVB light reflected and absorbed by human stratum corneum, along with the transmitted light to the dermis (Diffey, 1983). This constitutes the maximum percentage of the incident light that can be absorbed by the dermal tissue.

Besides the UV type, the magnitude of the maximum absorbed UV dosage into the dermis is also influenced by the relative melanin content in the epidermis (Diffey, 1983). To establish if relationships exist between changes in the mechanical properties of skin and the absorbed UV dosage, regression analyses are performed, employing relative melanin contents of 1 and 2, which represent the relative extremes of melanin content in human skin (Diffey, 1983). Fig. 7 shows linear regression analyses of fractional relative differences in the mechanical properties against absorbed energy dosage using a relative melanin content of 1, while Supplemental Fig. 3 employs a relative melanin content of 2 as a multiplication factor. The results highlight that while relative melanin content influences the magnitude of the maximum absorbed energy, it does not alter the fit of the linear regression. Simple linear regression and goodness of fit assessment analysis reveals a statistically significant relationship between the absorbed energy and the fractional relative difference in toughness (see Fig. 7B) and fracture stress (see Fig. 7C), suggesting that the described changes in mechanical properties scale with absorbed UV dosages. No statistically significant relationships between elastic modulus or fracture strain and the absorbed UV dosage exist however (Fig. 7A and D).

4.3. Effects of photoaging on collagen structure

Overall, UVA and UVB light can induce stiffening of full thickness skin along with increases in fracture stress and toughness (Fig. 6). Prior studies have demonstrated the ability of UV light to alter the structure of collagen gels, resulting in increases in their stiffness through cross-linking (Mitsuhashi et al., 2018; Rezakhaniha et al., 2012). Similarly, the observed changes in the mechanical properties of skin may be caused through structural changes in the dermal collagen fiber network, potentially through increased collagen fiber cross-linking. We, therefore, examine the effect of UV light on changes in the tissue's collagen microstructure.

Fig. 8A reveals a statistically significant rise in the fractional relative collagen fiber network density, $\Delta\rho/\rho_C = (\rho_{UV} - \rho_C)/\rho_C$, between samples irradiated with 1600 J/cm^2 of either UVA or UVB light and unirradiated controls. Collagen fiber density for UV irradiated samples is denoted as ρ_{UV}, while corresponding control fiber density is denoted as ρ_C. The differences in collagen density are more pronounced with UVA treated samples, potentially due to a greater transmission of this UV range into the dermal tissue (Diffey, 1983). The closer spacing of collagen fibers suggests increased crosslinking. This contrasts with prior studies that report UV irradiation of 30 J/cm^2 causes a depletion in collagen density near the epidermal-dermal junction (Liu et al., 2022), however, this study employed coronal sections, which cannot account for the orientation of the collagen in the section, which is likely to notably influence the fluorescent response. Increases in collagen density with UV exposure due to increased crosslinking could explain the observed changes in mechanical properties of skin shown in Fig. 6 A-C. However, we note UV irradiation does not notably impact the overall fracture strain, as shown in Fig. 6D. As such, studies exploring the tortuosity of collagen are performed next.

Fig. 8B shows that no significant changes in fractional relative collagen fiber tortuosity, $\Delta P/P_S = (Ps_{UV} - Ps_C)/Ps_C$, between UV irradiated samples and unirradiated controls occurs with either UVA or UVB irradiation, indicating that changes in density do not affect the undulated configuration of the fibers in the unloaded state. Here Ps_{UV} denotes

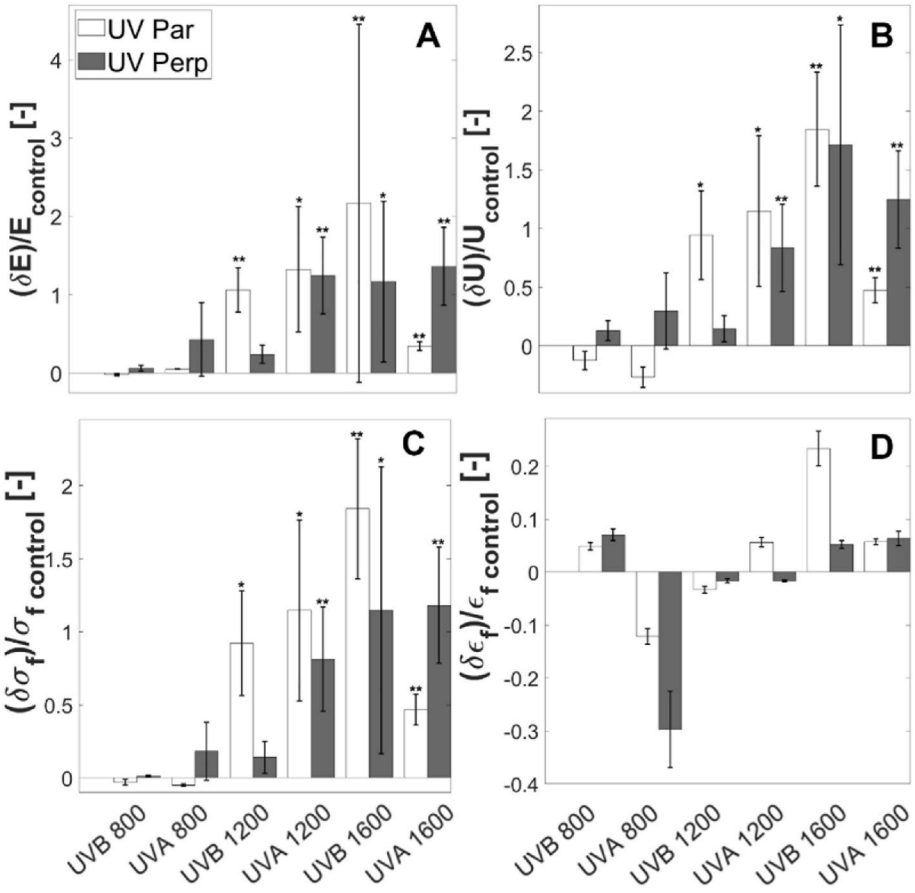

Fig. 6. Changes in the average fractional relative difference of A. elastic modulus, $(E_{UV} - E_C)/E_C$, B. toughness, $(U_{UV} - U_C)/U_C$, C. fracture stress, $(\sigma_{f,UV} - \sigma_{f,C})/\sigma_{f,C}$, and D. fracture strain, $(\varepsilon_{f,UV} - \varepsilon_{f,C})/\varepsilon_{f,C}$, with UVA and UVB irradiation. Samples excised parallel (Par, open bars) and perpendicular (Perp, filled bars) to the dominant collagen fiber orientation are shown. Bars denote average values of $3 \leq n \leq 5$ individual sample measurements for each range and dosage condition. Error bars denote the propagated uncertainty based on the standard deviations of the control and UV irradiated samples. *, **, and *** respectively note significance levels of $p < 0.05$, $p < 0.01$, and $p < 0.001$.

Table 2
Total UV light reflected, absorbed, and transmitted through human stratum corneum.

UV range	Reflected (%)	Absorbed (%)	Transmitted (%)
UVA (365 narrowband)	20	25	55
UVB (302 narrowband)	12	50	38

the average collagen fiber tortuosity of UV irradiated samples and Ps_C denotes the equivalent measurement for unirradiated control samples. The inset figure in Fig. 8B also shows average collagen fiber tortuosity, P, between UV irradiated samples (open bars) and their respective unirradiated controls (filled bars). This lack of change in collagen tortuosity is further verified by examining average relative fractional changes in the inflection point strain, $\Delta\varepsilon_i/\varepsilon_{i,C} = (\varepsilon_{i,UV} - \varepsilon_{i,C})/\varepsilon_{i,C}$, of the J-shaped stress-strain curves where $\varepsilon_{i,UV}$ denotes the inflection point strain of UV irradiated samples and $\varepsilon_{i,C}$ denotes the equivalent parameter for the unirradiated controls. The inflection point denotes the initial point of nonlinearity on the J-shaped stress-strain curve, prior to the onset of the second linear regime, where collagen fibers first become recruited (Yang et al., 2015). Fig. 8C reveals that no statistical difference in the inflection point strain occurs between UV irradiated samples and their corresponding controls, further indicating a lack of change in fiber tortuosity due to UV irradiation.

5. Research limitations

The ex-vivo human skin samples used in this study do not maintain the residual stress conditions that exist in skin in-vivo. Prior studies have shown that post excision, skin in an unloaded state deforms relative to its in-vivo dimensions with the greatest loss of tension aligned close to the direction of dominant collagen fiber orientation (Reihsner et al., 1995). We anticipate similar behavior for samples used in this study. As such, the samples employed will not accurately characterize in vivo stress conditions. However, this study maintains identical storage and testing conditions for the UV irradiated and corresponding control samples, permitting a justifiable comparison of the biomechanical changes resulting from prolonged UV exposure. Alongside biomechanical changes, skin structural and compositional changes are anticipated shortly following death of the donor (Wei et al., 2020). While structural and compositional changes can influence the biomechanical properties of the skin tissue, a majority of the initial changes observed occur in the very thin epidermal layers, which constitutes less than 10% volume of a full thickness skin tissue (Kuwazuru et al., 2008; Venus et al., 2010). The UV treated and corresponding control samples used in this study are excised from the same donor and stored for similar time periods, again permitting justifiable comparisons of changes in structure and composition. Lastly, this study does not evaluate the structural and directional influence of dermal elastin fibers. The primary justification for this decision was the greater mass and presence of dermal collagen fibers per unit volume compared to dermal elastin fibers (Brown TM and Krishnamurthy K, 2021), playing a more dominant role in influencing the toughness and stiffness characteristics of full thickness tissue within and beyond the second linear regime (Aziz et al., 2016).

6. Conclusion

While prior studies have noted enzymatic induced physiological changes to the skin resulting from changes in dermal fibroblast activity as a result of UV radiation (Cho et al., 2009; Chung et al., 2002; Fisher et al., 1996; Kappes et al., 2006; Kollias and Baqer, 1984; Lee et al., 2006), no study until now has explored the biomechanical effects of UV

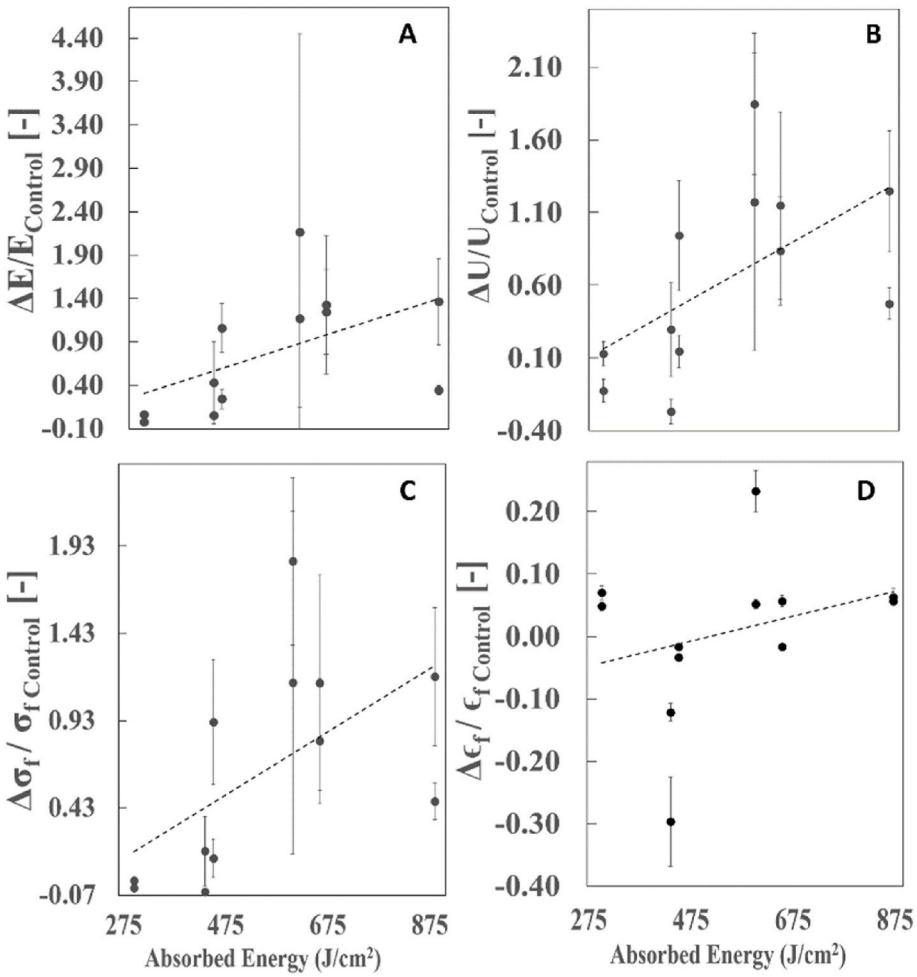

Fig. 7. Fractional relative difference of mechanical properties as a function of maximum absorbed energy. Results include both changes in the fractional relative elastic modulus (A), toughness (B), fracture stress (C), and fracture strain (D) of samples with collagen fibers aligned and perpendicular to the loading axis. The best fit line has $R^2 = 0.279$ for elastic modulus, $R^2 = 0.335$ for toughness, $R^2 = 0.338$ for fracture stress, and $R^2 = 0.103$ for fracture strain. Goodness of fit assessment shows $p = 0.07$ for elastic modulus, $p = 0.04$ for toughness, $p = 0.04$ for fracture stress, and $p = 0.32$ for fracture strain. Calculations for the absorbed energy ranges assume a relative melanin content of 1.

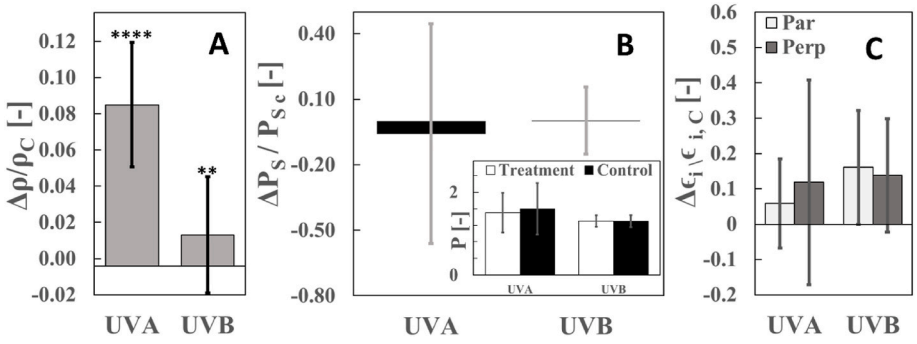

Fig. 8. Changes in the average fractional relative difference of A. collagen density, $(\rho_{UV}-\rho_C)/\rho_C$, B. collagen tortuosity, $(Ps_{UV}-Ps_C)/Ps_C$ and average collagen tortuosity, P (inset) and C. inflection point strain, $(\varepsilon_{i,UV}-\varepsilon_{i,C}/\varepsilon_{i,C})$ between samples irradiated with UVA and UVB 1600 J/cm^2, and their respective controls. The inset figure in panel B shows the average UV treated collagen tortuosity (Treatment, open bars), P, along with the respective control (Control, filled bars). In panel C, samples excised parallel (Par, filled bars, light grey)) and perpendicular (Perp, filled bar, light black) to the dominant collagen fiber orientation are shown. Error bars denote the propagated uncertainty based on the standard deviations of the control and UV irradiated samples. *, **, ***, and **** respectively note significance levels of $p < 0.05$, $p < 0.01$, $p < 0.001$, and $p < 0.0001$.

radiation on full thickness human skin, or established changes to the mechanical-microstructural relationships caused by UV light. In this study, we have quantified mechanical changes in full thickness human skin due to UVA and UVB irradiation while accounting for the anisotropic collagen orientation and mechanical properties of the tissue. UV induced mechanical changes are also linked to microstructural changes in the collagen fiber network. The mechanical testing data in this study reveals that with sufficient incident dosages of UVA and UVB light, changes in the elastic modulus, toughness, and fracture stress of full-thickness skin occur when comparing UV treated samples with controls. While this agrees with prior studies that report increases in UV induced collagen stiffness in hydrogels and matrices (Lee et al., 2001; Tirella et al., 2012), similar changes have not to date been reported in human tissue directly. Further, this study correlates observed mechanical changes with an increase in collagen fiber bundle density with sufficient incident dosages of both UVA and UVB light. Prior studies reporting a correlation between collagen concentration and stiffness profile in collagen gels (Roeder et al., 2002; Tirella et al., 2012) further support these mechanical-structural relationship changes. No significant changes in collagen fiber tortuosity between the UV treated and its counterpart control samples exist however, further supported by a lack of change to the inflection point of the J-shaped stress strain curves and

the fracture strain of the tissue. Results also indicate that the absorbed UV dosage, irrespective of the incident UV range governs changes to the toughness and fracture stress of the tissue.

This study primarily sourced skin specimens from photoprotected anatomical regions. Prior studies have reported differences in the biomechanical properties (Lynch et al., 2022) and melanin content (Firooz et al., 2012) between skin from photoprotected and photo-exposed anatomical sites. We anticipate the mechanical and structural changes reported will become reduced for photoexposed skin due to increased melanin content offering improved photoprotection (Diffey, 1983).

This study also elucidates a new technique to characterize the dominant collagen fiber orientation in excised human skin specimens without prior knowledge of the skin tension lines, anatomical site or in-vivo orientation of the skin specimens. Previously, an understanding of the anisotropic mechanical properties of human skin required knowledge of the location and orientation of the samples prior to excision (Ní Annaidh et al., 2012). We anticipate that this technique could be employed to better understand the anisotropic behavior of other soft and hard biological materials including cardiac (Kotadia et al., 2020), brain (Budday et al., 2017; Feng et al., 2013), and bone tissue (Kang et al., 2020).

Prior studies noting molecular changes in dermal tissue as a result of UV irradiation have primarily been done using electrophoresis or polymerase chain reaction (Cho et al., 2009; Chung et al., 2002; Fisher et al., 1996; Kappes et al., 2006; Kollias and Baqer, 1984; Lee et al., 2006). While such measurements can detect and reveal changes at a genetic or molecular level, it remains unclear how these changes will manifest into the structural characteristics of collagen fiber bundles and could be a topic of future research.

Future work should explore methods of detecting and measuring collagen crosslinking in skin and other biological tissues. While this study observes a rise in collagen density and relates this structural change to the rise in the mechanical toughness of skin, it is hard to definitively explain the increased collagen density. We conjecture that increased density could be due to collagen crosslinking with UV radiation observed in previous studies; however, these studies did not measure these changes in biological tissues and future work can validate this hypothesis (Lee et al., 2001; Tirella et al., 2012).

CRediT authorship contribution statement

Abraham Ittycheri: Writing – review & editing, Writing – original draft, Visualization, Validation, Methodology, Investigation, Formal analysis, Data curation. **Zachary W. Lipsky:** Writing – review & editing, Validation, Methodology, Investigation, Formal analysis, Data curation. **Tracy A. Hookway:** Writing – review & editing, Writing – original draft. **Guy K. German:** Writing – review & editing, Writing – original draft, Supervision, Resources, Project administration, Methodology, Investigation, Funding acquisition, Formal analysis, Conceptualization.

Declaration of competing interest

The authors declare that they have no known competing financial interests or personal relationships that could have appeared to influence the work reported in this paper.

Data availability

The data will upon acceptance of the article, be placed in the Open Repository @Binghamton (ORB)

Acknowledgements

This material is based upon work supported by the National Science Foundation under grant no. 1653071.

Appendix A. Supplementary data

Supplementary data to this article can be found online at https://doi.org/10.1016/j.jmbbm.2023.105880.

References

Amaro-Ortiz, A., Yan, B., D'Orazio, J.A., 2014. Ultraviolet radiation, aging and the skin: prevention of damage by topical cAMP manipulation. Molecules. https://doi.org/10.3390/molecules19056202.

Aziz, J., Shezali, H., Radzi, Z., Yahya, N.A., Abu Kassim, N.H., Czernuszka, J., Rahman, M.T., 2016. Molecular mechanisms of stress-responsive changes in collagen and elastin networks in skin. Skin Pharmacol. Physiol. 29, 190–203. https://doi.org/10.1159/000447017.

Böni, R., Schuster, C., Nehrhoff, B., Burg, G., 2002. Epidemiology of skin cancer. Neuroendocrinol. Lett. 23 (Suppl. 2), 48–51.

Brown, S.R., Melman, L., Jenkins, E., Deeken, C., Frisella, M.M., Brunt, L.M., Eagon, J.C., Matthews, B.D., 2011. Collagen type I:III ratio of the gastroesophageal junction in patients with paraesophageal hernias. Surg. Endosc. 25, 1390–1394. https://doi.org/10.1007/s00464-010-1373-7.

Brown, T.M., Krishnamurthy, K., 2021. Histology, Dermis. StatPearls Publishing.

Budday, S., Sommer, G., Birkl, C., Langkammer, C., Haybaeck, J., Kohnert, J., Bauer, M., Paulsen, F., Steinmann, P., Kuhl, E., Holzapfel, G.A., 2017. Mechanical characterization of human brain tissue. Acta Biomater. 48, 319–340. https://doi.org/10.1016/j.actbio.2016.10.036.

Chandler, S., Cossins, J., Lury, J., Wells, G., 1996. Macrophage metalloelastase degrades matrix and myelin proteins and processes a tumour necrosis factor-alpha fusion protein. Biochem. Biophys. Res. Commun. 228, 421–429. https://doi.org/10.1006/bbrc.1996.1677.

Chavoshnejad, P., Foroughi, A.H., Dhandapani, N., German, G.K., Razavi, M.J., 2021. Effect of collagen degradation on the mechanical behavior and wrinkling of skin. Phys. Rev. E 104, 034406. https://doi.org/10.1103/PhysRevE.104.034406.

Cho, S., Shin, M.H., Kim, Y.K., Seo, J.E., Lee, Y.M., Park, C.H., Chung, J.H., 2009. Effects of infrared radiation and heat on human skin aging in vivo. In: Journal of Investigative Dermatology Symposium Proceedings. Nature Publishing Group, pp. 15–19. https://doi.org/10.1038/jidsymp.2009.7.

Chung, J.H., Seo, J.Y., Lee, M.K., Eun, H.C., Lee, J.H., Kang, S., Fisher, G.J., Voorhees, J. J., 2002. Ultraviolet modulation of human macrophage metalloelastase in human skin in vivo. J. Invest. Dermatol. 119, 507–512. https://doi.org/10.1046/j.1523-1747.2002.01844.x.

Diffey, B.L., 1983. A mathematical model for ultraviolet optics in skin. Phys. Med. 28, 647–657. https://doi.org/10.1088/0031-9155/28/6/005.

Feng, Y., Okamoto, R.J., Namani, R., Genin, G.M., Bayly, P. v, 2013. Measurements of mechanical anisotropy in brain tissue and implications for transversely isotropic material models of white matter. J. Mech. Behav. Biomed. Mater. 23, 117–132. https://doi.org/10.1016/j.jmbbm.2013.04.007.

Firooz, A., Sadr, B., Babakoohi, S., Sarraf-Yazdy, M., Fanian, F., Kazerouni-Timsar, A., Nassiri-Kashani, M., Naghizadeh, M.M., Dowlati, Y., 2012. Variation of biophysical parameters of the skin with age, gender, and body region. Sci. World J. 1–5. https://doi.org/10.1100/2012/386936, 2012.

Fisher, G.J., Datta, S.C., Talwar, H.S., Wang, Z.-Q., Varani, J., Kang, S., Voorhees, J.J., 1996. Molecular basis of sun-induced premature skin ageing and retinoid antagonism. Nature 379, 335–339. https://doi.org/10.1038/379335a0.

Freeman, S., Kibler, K., Lipsky, Z., Jin, S., German, G.K., Ye, K., 2022. Systematic evaluating and modeling of SARS-CoV-2 UVC disinfection. Sci. Rep. 12 https://doi.org/10.1038/s41598-022-09930-2.

Gasperini, A.E., Sanchez, S., Doiron, A.L., Lyles, M., German, G.K., 2017. Non-ionising UV light increases the optical density of hygroscopic self assembled DNA crystal films. Sci. Rep. 7, 6631. https://doi.org/10.1038/s41598-017-06884-8.

Griffin, M.F., Leung, B.C., Premakumar, Y., Szarko, M., Butler, P.E., 2017. Comparison of the mechanical properties of different skin sites for auricular and nasal reconstruction. Int. J. Otolaryngol. Head Neck Surg. 46, 33. https://doi.org/10.1186/s40463-017-0210-6.

Junqueira, L.C., Bignolas, G., Brentani, R.R., 1979. Picrosirius staining plus polarization microscopy, a specific method for collagen detection in tissue sections. Histochem. J. 11, 447–455. https://doi.org/10.1007/BF01002772.

Kang, J., Dong, E., Li, D., Dong, S., Zhang, C., Wang, L., 2020. Anisotropy characteristics of microstructures for bone substitutes and porous implants with application of additive manufacturing in orthopaedic. Mater. Des. 191 https://doi.org/10.1016/j.matdes.2020.108608.

Kappes, U.P., Luo, D., Potter, M., Schulmeister, K., Rü Nger, T.M., 2006. Short- and long-wave UV light (UVB and UVA) induce similar mutations in human skin cells. J. Invest. Dermatol. 126, 667–675. https://doi.org/10.1038/sj.jid.5700093.

Kollias, N., Baqer, A., 1984. An experimental study of the changes in pigmentation in human skin in V N O with visible and near infrared light. Photochem. Photobiol. 39, 651–659. https://doi.org/10.1111/j.1751-1097.1984.tb03905.x.

Kotadia, I., Whitaker, J., Roney, C., Niederer, S., O'Neill, M., Bishop, M., Wright, M., 2020. Anisotropic cardiac conduction. Arrhythmia Electrophysiol. Rev. 9, 202–210. https://doi.org/10.15420/aer.2020.04.

Kuwazuru, O., Saothong, J., Yoshikawa, N., 2008. Mechanical approach to aging and wrinkling of human facial skin based on the multistage buckling theory. Med. Eng. Phys. 30, 516–522. https://doi.org/10.1016/j.medengphy.2007.06.001.

Langer, K., 1861. On the anatomy and physiology of the skin. II. Skin tension by Professor K. Langer, presented at the meeting of 27th November 1861. In: British Journal of Plastic Surgery.

Lee, C.R., Grodzinsky, A.J., Spector, M., 2001. The effects of cross-linking of collagen-glycosaminoglycan scaffolds on compressive stiffness, chondrocyte-mediated contraction, proliferation and biosynthesis. Biomaterials 22, 3145–3154. https://doi.org/10.1016/s0142-9612(01)00067-9.

Lee, J.H., Roh, M.R., Lee, K.H., 2006. Effects of infrared radiation on skin photo-aging and pigmentation. Yonsei Med. J. 47, 485–490. https://doi.org/10.3349/ymj.2006.47.4.485.

Liang, X., Boppart, S.A., 2010. Biomechanical properties of in vivo human skin from dynamic optical coherence elastography. IEEE Trans. Biomed. Eng. 57, 953–959. https://doi.org/10.1109/TBME.2009.2033464.

Lipsky, Z.W., German, G.K., 2019. Ultraviolet light degrades the mechanical and structural properties of human stratum corneum. J. Mech. Behav. Biomed. Mater. 100 https://doi.org/10.1016/j.jmbbm.2019.103391.

Liu, Y., Liu, J., Dai, H., Wang, R., Hsiao, A., Wang, W., Betts, R.J., Marionnet, C., Bernerd, F., Qiu, J., 2022. Photo-aging evaluation - in vitro biological endpoints combined with collagen density assessment with multi-photon microscopy. J. Dermatol. Sci. 105, 37–44. https://doi.org/10.1016/j.jdermsci.2021.12.002.

Lynch, B., Pageon, H., le Blay, H., Brizion, S., Bastien, P., Bornschlögl, T., Domanov, Y., 2022. A mechanistic view on the aging human skin through ex vivo layer-by-layer analysis of mechanics and microstructure of facial and mammary dermis. Sci. Rep. 12 https://doi.org/10.1038/s41598-022-04767-1.

Meijering, E., Jacob, M., Sarria, J.-C.F., Steiner, P., Hirling, H., Unser, M., 2004. Design and validation of a tool for neurite tracing and analysis in fluorescence microscopy images. Cytometry 58, 167–176. https://doi.org/10.1002/cyto.a.20022.

Mitsuhashi, K., Ghosh, S., Koibuchi, H., 2018. Mathematical modeling and simulations for large-strain J-shaped diagrams of soft biological materials. Polymers 10. https://doi.org/10.3390/polym10070715.

Moan, J., Carmen Porojnicu, A., Dahlback, A., Setlow, R.B., 2008. Addressing the health benefits and risks, involving vitamin D or skin cancer, of increased sun exposure. PNAS 105, 668–673. https://doi.org/10.1073/pnas.0710615105.

Morita, A., Werfel, T., Stege, H., Ahrens, C., Karmann, K., Grewe, M., Grether-Beck, S., Ruzicka, T., Kapp, A., Klotz, L.O., Sies, H., Krutmann, J., 1997. Evidence that singlet oxygen-induced human T helper cell apoptosis is the basic mechanism of ultraviolet-A radiation phototherapy. J. Exp. Med. 186, 1763–1768. https://doi.org/10.1084/jem.186.10.1763.

Ní Annaidh, A., Bruyère, K., Destrade, M., Gilchrist, M.D., Otténio, M., 2012. Characterization of the anisotropic mechanical properties of excised human skin. J. Mech. Behav. Biomed. Mater. 5, 139–148. https://doi.org/10.1016/j.jmbbm.2011.08.016.

Panich, U., Sittithumcharee, G., Rathviboon, N., Jirawatnotai, S., 2016. Ultraviolet radiation-induced skin aging: the role of DNA damage and oxidative stress in epidermal stem cell damage mediated skin aging. Stem Cell. Int. https://doi.org/10.1155/2016/7370642.

Poon, F., Kang, S., Chien, A.L., 2015. Mechanisms and treatments of photoaging. Photodermatol. Photoimmunol. Photomed. 31, 65–74. https://doi.org/10.1111/phpp.12145.

Reihsner, R., Balogh, B., Menzel, E.J., 1995. Two-dimensional elastic properties of human skin in terms of an incremental model at the in vivo configuration. Med. Eng. Phys. 17, 304–313. https://doi.org/10.1016/1350-4533(95)90856-7.

Reynolds, N.J., Franklin, V., Gray, J.C., Diffey, B.L., Farr, P.M., 2001. Narrow-band ultraviolet B and broad-band ultraviolet A phototherapy in adult atopic eczema: a randomised controlled trial. Lancet 357. https://doi.org/10.1016/S0140-6736(00)05114-X, 2012–6.

Rezakhaniha, R., Agianniotis, A., Schrauwen, J.T.C., Griffa, A., Sage, D., Bouten, C.V.C., van de Vosse, F.N., Unser, M., Stergiopulos, N., 2012. Experimental investigation of collagen waviness and orientation in the arterial adventitia using confocal laser scanning microscopy. Biomech. Model. Mechanobiol. 11, 461–473. https://doi.org/10.1007/s10237-011-0325-z.

Ridge, M.D., Wright, V., 1966. The directional effects of skin. A bio-engineering study of skin with particular reference to Langer's lines. J. Invest. Dermatol. 46, 341–346. https://doi.org/10.1038/jid.1966.54.

Roeder, B.A., Kokini, K., Sturgis, J.E., Robinson, J.P., Voytik-Harbin, S.L., 2002. Tensile mechanical properties of three-dimensional type I collagen extracellular matrices with varied microstructure. J. Biomech. Eng. 124, 214–222. https://doi.org/10.1115/1.1449904.

Schatrffetter-Kochanek, K., 1996. Photoaging of the connective tissue of skin: its prevention and therapy. Adv. Pharmacol. 38, 639–655. https://doi.org/10.1016/s1054-3589(08)61003-0.

Silver, F.H., Freeman, J.W., DeVore, D., 2001. Viscoelastic properties of human skin and processed dermis. Skin Res. Technol. 7, 18–23. https://doi.org/10.1034/j.1600-0846.2001.007001018.x.

Tirella, A., Liberto, T., Ahluwalia, A., 2012. Riboflavin and collagen: new crosslinking methods to tailor the stiffness of hydrogels. Mater. Lett. 74, 58–61. https://doi.org/10.1016/j.matlet.2012.01.036.

United Nations Environment Programme, 1998. Environmental Effects of Ozone Depletion : 1998 Assessment : Pursuant to Article 6 of the Montreal Protocol on Substances that Deplete the Ozone Layer. UNEP.

Venus, M., Waterman, J., McNab, I., 2010. Basic physiology of the skin. Surgery 28, 469–472. https://doi.org/10.1016/j.mpsur.2010.07.011.

Vierkötter, A., Krutmann, J., 2012. Environmental influences on skin aging and ethnic-specific manifestations. Dermatoendocrinol 4, 227–231. https://doi.org/10.4161/derm.19858.

Wei, W., Michu, Q., Wenjuan, D., Jianrong, W., Zhibing, H., Ming, Y., Bo, J., Xia, L., 2020. Histological changes in human skin 32 days after death and the potential forensic significance. Sci. Rep. 10, 18753 https://doi.org/10.1038/s41598-020-76040-2.

Welgus, H.G., Campbell, E.J., Bar-Shavit, Z., Senior, R.M., Teitelbaum, S.L., 1985. Human alveolar macrophages produce a fibroblast-like collagenase and collagenase inhibitor. J. Clin. Invest. 76, 219–224. https://doi.org/10.1172/JCI111949.

Wilkes, G.L., Brown, I.A., Wildnauer, R.H., 1973. The biomechanical properties of skin. CRC Crit. Rev. Bioeng. 1, 453–495.

Yang, W., Sherman, V.R., Gludovatz, B., Schaible, E., Stewart, P., Ritchie, R.O., Meyers, M.A., 2015. On the tear resistance of skin. Nat. Commun. 6, 6649. https://doi.org/10.1038/ncomms7649.

Yu, Q., Chen, Y., Xu, C.-B., 2017. A convenient method for quantifying collagen fibers in atherosclerotic lesions by ImageJ software. Int. J. Clin. Exp. Med 10, 14904–14910.